Spatial variation of microstructure and petrophysical properties along deformation bands in reservoir sandstones

Anita Torabi and Haakon Fossen

ABSTRACT

A series of deformation bands from various reservoir sandstones deformed at different burial depths have been studied with respect to microstructural and petrophysical variations. In many of the examples explored, the internal microstructure, porosity, and permeability vary along the bands at the centimeter or even millimeter scale, changing and in most cases reducing the ability of the bands to act as barriers to fluid flow. Porosity varies by up to 18% and permeability by up to two orders of magnitude. Such petrophysical variations are found along different types of deformation bands, but the range depends upon the deformation mechanisms, in particular on the degree of cataclasis and dissolution in cataclastic and dissolution bands, and on the phyllosilicate content in disaggregation bands. For cataclastic bands, the grain-size distribution changes along the bands with regard to the degree of cataclasis. Furthermore, the increased specific surface area of the pore-grain interface as a result of cataclasis causes higher permeability reduction in cataclastic bands than in other types of deformation bands. Phyllosilicate content can influence the thickness of phyllosilicate bands. However, no apparent correlation between thickness and intensity of cataclasis in the studied cataclastic deformation bands is observed.

Manuscript received December 3, 2008; provisional acceptance February 3, 2009; revised manuscript received March 13, 2009; final acceptance March 27, 2009.
DOI:10.1306/03270908161

AUTHORS

ANITA TORABI ~ *Centre for Integrated Petroleum Research, Unifob Petroleum, University of Bergen, Post Box 7800, 5020 Bergen, Norway; anita.torabi@cipr.uib.no*

Anita Torabi received her B.S. degree in geology from the University of Tehran (1993) and her Ph.D. in petroleum structural geology from the University of Bergen (2008). She joined the Center for Integrated Petroleum Research at the University of Bergen in 2004 and is currently a senior researcher. Her scientific interests include the analysis of faulted and fractured reservoirs in different stress regimes, fault-related folding and its role in hydrocarbon entrapment, and the effect of faulting on the petrophysical properties of rocks and fluid flow.

HAAKON FOSSEN ~ *Centre for Integrated Petroleum Research/Department of Earth Science, University of Bergen, Post Box 7800, 5020 Bergen, Norway; Haakon.Fossen@geo.uib.no*

Haakon Fossen received his Candidatus Scientiarum (M.S. degree equivalent) degree from the University of Bergen (1986) and his Ph.D. in structural geology from the University of Minnesota (1992). He joined Statoil in 1986 and, since 1996, has been a professor in structural geology at the University of Bergen. His scientific interests cover the evolution and collapse of mountain ranges, the structure of rift basins, and petroleum-related deformation structures at various scales.

ACKNOWLEDGEMENTS

We are grateful to the sponsors of the Fault Facies project (Norwegian Research Council, StatoilHydo, and Conoco-Philips) at the Center for Integrated Petroleum Research at the University of Bergen. Thanks to Behzad Alaei for scientific advice in the image processing work. Alvar Braathen, Gretchen M. Gillis, Stephen Naruk, Richard H. Worden, Joachim E. Amthor, and Terrilyn M. Olson are thanked for critically commenting on a previous version of the manuscript. We are grateful to Frances P. Whitehurst for her comments on the latest version of the manuscript.
The AAPG Editor thanks the following reviewers for their work on this paper: Steven M. Goolsby, Steve Hansen, and Terrilyn M. Olson.

EDITOR'S NOTE

Color versions of Figures 1–6 may be seen in the online version of this article.

INTRODUCTION

Deformation bands are localized deformation structures that form in highly porous rocks and sediments. They are commonly found in faulted sand and reservoir-quality sandstone (e.g., Aydin, 1978; Pittman, 1981; Jamison and Stearns, 1982; Underhill and Woodcock, 1987; Knipe et al., 1997; Fossen et al., 2007), and their internal characteristics have the potential to greatly change the petrophysical properties of reservoirs and thus affect the choice of production strategy of oil and gas fields (Fisher and Knipe, 2001; Hesthammer and Fossen, 2001; Ogilvie and Glover, 2001).

Deformation bands form by different deformation mechanisms (Fossen et al., 2007). Disaggregation bands result from granular flow that involves rolling, sliding, and rotation of sand grains. These bands do not commonly affect the petrophysical properties of sandstone reservoirs significantly (e.g., Fossen et al., 2007) unless the phyllosilicate content exceeds 10–15%. In this case, the phyllosilicate minerals align along the band, and the term phyllosilicate band is applied (Knipe et al., 1997). Phyllosilicate bands can cause up to several orders of reduction in permeability according to plug measurements reported by Fisher and Knipe (2001). Cataclastic bands are characterized by grain fracture, crushing, and abrasion (cataclasis). Individual cataclastic bands are typically reported to reduce porosity of the deformed sandstone by one and permeability by three orders of magnitude as compared to their host rock (e.g., Antonellini and Aydin, 1994). Dissolution and cementation bands form where dissolution or cementation is the dominant deformation mechanism. A dissolution band typically consists of tightly packed quartz grains with little or no indication of grain fracture (Gibson, 1998). Quartz dissolution and cementation have been invoked to explain poor reservoir performance in North Sea reservoirs located at greater than 3-km (1.8-mi) depth (Hesthammer et al., 2002).

Single deformation bands in the outcrop are typically about 1 mm (0.03 in.) thick and up to 100 m (328 ft) long but can form clusters in which faults (slip surfaces) can initiate, as envisaged by Aydin and Johnson (1978). Clusters of bands can accumulate several hundred bands over a zone less than a meter wide (Johansen and Fossen, 2008), in which case the zone can be several hundred meters long. They can also form and grow in the damage zone of an existing fault, for instance as a response to geometric complications during fault slippage (e.g., Rykkelid and Fossen, 2002).

Because deformation bands and deformation band zones are long enough to compartmentalize reservoirs, several previous workers (e.g., Aydin, 1978; Pittman, 1981; Jamison and Stearns, 1982; Underhill and Woodcock, 1987; Knipe et al., 1997; Gibson, 1998; Fisher and Knipe, 2001) devoted attention to their physical properties. However, variations in porosity and permeability, related to microstructural variations within deformation bands, have been given little or no attention in the existing literature (cf. Fossen and Bale, 2007). The typical reported cataclastic deformation bands of the Colorado Plateau, as described by Aydin, (1978), Aydin and Johnson (1978, 1983), and Davis (1999), form where mechanical grain fracture is the dominant deformation mechanism. These authors described deformation bands as consisting of a central cataclastic core within a volume of compacted rock, and the variation of microstructure across the band has also been studied through experimental work (e.g., Agung et al., 2004). Sharp boundary shear zones produced at a high level of stress in ring-shear experiments (Torabi et al., 2007) show zonation comparable to the microstructural variation reported by Aydin (1978). In these experiments, porosity across the bands ranged from about 24% in the host rock down to about 17% in the margin and to about 12% within the central part of the shear zone (Torabi et al., 2007). However, variations in microstructure along deformation bands have not been addressed before. Whether such variations generate changes in petrophysical properties along the bands and how they affect fluid flow in petroleum reservoirs are topics that will be assessed in this article.

Although microstructural variations along as well as across deformation bands are easily studied under a microscope, their internal permeability

structure is difficult to assess by means of classical methods. In general, image processing methods can be used to characterize the microstructure of rocks and provide a quantitative means for understanding the dependence of physical properties on pore structure (Ehrlich et al., 1984; Koplik and Vermette, 1984; Wissler, 1987; Doyen, 1988; Blair et al., 1996; Bakke and Øren, 1997; Keehm et al., 2004, 2006; White et al., 2006). In this study, we use an image processing method especially designed for the purpose of estimating porosity and permeability within deformation bands (Torabi et al., 2008). To see the effect of grain size on the microstructure of the bands, we describe the grain-size distributions in the measured locations in the host rock and within the bands. We first exemplify different types of deformation bands with respect to their deformation mechanism from different localities around the world (formed at different burial depth and tectonic setting) that show variations in thickness and microstructure along the band, and then present a case study from the Entrada Sandstone (Utah) to show variations along deformation bands as they cross layers of different grain size and porosity.

METHODOLOGY

Traditional permeability measurements using an inch-size plug for laboratory testing and minipermeameter in the field are hampered by large uncertainties and difficulties related to both sampling and measurements. Moreover, the resolution of plug measurements is constrained by the plug length and diameter (commonly 2.54 cm [1 in.]), whereas deformation structures such as single deformation bands in porous sandstones are only around 1 mm (0.03 in.) thick (Torabi et al., 2008). Therefore, laboratory-based plug measurements represent the effective permeability across a 2.54-cm (1-in.)-long sample, which includes a deformation band and its host rock. However, the image processing method applied here provides a means to estimate the porosity and permeability of deformation bands on the microscale and to map out the variations in properties along as well as across deformation bands. By using this method, we eliminate the size limitation on the porosity and permeability estimations of deformation bands imposed by traditional approaches. In this project, we have studied polished thin sections of faulted sandstones using optical and scanning electron microscopy. The samples are oriented perpendicular to deformation bands in the outcrop. High-resolution photomicrographs from optical microscope and backscattered electron (BSE) images of thin sections have been used for processing and estimating the porosity and permeability of the selected locations (small areas, see the specification in the following) of thin sections.

The locations selected for this study are represented schematically by points on the photomicrographs of the thin sections in the figures. Porosity and permeability have been estimated using spatial correlation functions and a modified version of the Kozeny-Carman relation (Torabi et al., 2008). To estimate porosity, low-magnification photomicrographs (1× and 2×) that cover the whole area of interest of both deformation bands and host rock have been used. Low-magnification images (images covering 10–100 grains) can cover an area over which measurements can be made that will yield a representative of the whole, and the estimated porosity values from these images are in agreement with porosity measured in the laboratory (Blair et al., 1996). For the process of permeability calculation, higher magnification (from 155× to 2580×) and resolution (1024 × 768) BSE images have been used. The choice of magnification for the images depends on the grain size; hence, the area of the used images varies from sample to sample. The procedure of the applied image-based processing, which has been developed in a function in MATLAB, is presented below.

First, a binary image from the selected high-resolution gray-scale image is made by choosing an appropriate threshold. The binary image $f_{(i,j)}$ is represented by an $M \times N$ matrix and is reversed to have 0 pixel value in the grain space and 1 in the pore space. The one-point correlation function (S_1, equation 1) (Garboczi et al., 1999), which gives information about the volume fraction of the

two phases (pore and grain), is applied to the binary image

$$S_1 = \phi = < f_{(i,j)} > = \frac{1}{M \times N} \sum_{ij} f_{(i,j)} \qquad i = 1, 2, \ldots M; \qquad j = 1, 2, \ldots N \tag{1}$$

This function gives the porosity (ϕ). The next step is to calculate the pore-pore two-point correlation function $S_2(x, y)$ for a selected binary image using equation 2, which is the probability that two points with a specified distance apart (a line) are both in pore phase (e.g., Berryman, 1985). The calculated two-point correlation function in the Cartesian coordinate system is then used to calculate the planar radial average in the polar coordinate system using a two-dimensional bilinear interpolation method.

$$S_2(x, y) = < f_{(i,j)} f_{(i+x,j+y)} > = \frac{1}{M \times N} \sum f_{(i,j)} f_{(i+x,j+y)} \tag{2}$$

The specific surface area (s, i.e., the total area of the pores divided by the total volume of the porous media, equation 3) of the pore-grain interface is calculated from the two-point correlation function (Berryman, 1998). High-magnification images that contain only a few grains are suitable for calculating a two-point correlation function and hence the estimated specific surface area (Blair et al., 1996). To capture the complex microgeometry of the deformation bands and its wide range of grain size, several high-magnification images need to be taken across the band to cover the entire width of the band. The average specific area is then calculated using specific surface areas obtained from the processing of these images (Torabi et al., 2008).

We calculated permeability using a modified version of the Kozeny-Carman relation (equation 4), where k is the permeability, ϕ is the porosity, c is a constant related to pore geometry that is equal to 2 for porous materials assuming circular cross section for pores, and F is the formation factor and has an exponential relationship with porosity (Archie, 1942, equation 5). In this relation, the exponent m is a cementation factor and it ranges between 1.5 for poorly consolidated sandstones and 2 for well consolidated sandstones (Brace, 1977; Sen et al., 1981; Wong et al., 1984, Blair et al., 1996). We have assumed exponent m to be equal to 1.8 for our moderately consolidated sandstones.

$$S_2'(0) = -s/4 \tag{3}$$

$$k = \phi^2 / cFs^2 \tag{4}$$

$$F = \phi^{-m} \tag{5}$$

Grain-size distributions have been analyzed from the binary version of high-resolution BSE images using ImageJ software. The obtained grain-size areas (GSA on the plots of grain-size distribution) were calibrated in square micrometers by setting the real scale on the images. The grain-size distributions are presented as exceedance frequency (EF) plots for all the thin sections. The EF of a particular value of a measured variable is defined as the number of data with values greater than that value, divided by the total number of the values (e.g., Torabi et al., 2007).

RESULTS FROM THE THIN-SECTION STUDY

In this section, we quantify the spatial variation of grain size, porosity, and permeability within deformation bands through a microstructural study. Our samples consist of different types of deformation bands associated with different deformation mechanisms from different localities around the world. Special attention has been devoted to deformation bands from the Entrada Sandstone, Utah, to study the effect of initial grain size and porosity on the properties of the bands where they cross different lithologic layers (Table 1).

Deformation Bands and Deformation Mechanisms

Deformation mechanisms in porous sand and sandstones depend on factors such as mineralogy, grain size, shape, sorting, cementation, porosity,

Table 1. Description of the Samples Used in this Study

Sample	Mineralogy	Type of Band	Diagenetic Features	Formation	Location
3701	–	Phyllosilicate and disaggregation band	–	Brent Group	North Sea, Huldra field
UT-A	Quartz arenite	Dissolution band	Quartz dissolution	Entrada Sandstone	San Rafael Desert, Utah
LD-6A1	Quartz arenite	Cataclastic band	Some iron oxide	Nubian Sandstone	Sinai, Egypt
LD-6A2	Quartz arenite	Cataclastic band	Some iron oxide	Nubian Sandstone	Sinai, Egypt
WK-13	Quartz arenite	Cataclastic band	–	Nubian Sandstone	Sinai, Egypt
MC-1–9	Litharenite	Cataclastic bands	Some iron oxide in MC-6, MC-7	Entrada Sandstone	San Rafael Desert, Utah

and state of stress and strain (Fossen et al., 2007). Different mechanisms produce bands with different petrophysical properties, and the primary mechanisms are (1) granular flow, (2) cataclasis, and (3) dissolution and cementation. In general, granular flow characterizes the deformation of sand and sandstone at shallow depths.

Figure 1a shows a deformation band formed by granular flow, characterized as a phyllosilicate band on the right side of the image (sample 3701). The sandstone sample was taken from the Brent Group in the North Sea Huldra field (Fossen et al., 2003). The sample is from 3701-m (12,142-ft) depth but formed at less than a few hundred meters burial during Late Jurassic North Sea rifting. Changes in porosity and permeability are observed both along and across the band as its phyllosilicate (mica) content varies (Figure 1a); the phyllosilicate content is so low in the left half of the band that the band is difficult to trace. Apparently, the band is thicker in the right part where the phyllosilicate content is high.

The highest porosity and permeability values (21% and 210 md, respectively) were obtained in the host rock where the phyllosilicate content is low and within the left (nonphyllosilicate) part of the band (22% and 133 md). Hence, little or no porosity and permeability contrast exists between the band and the host rock in the left part of sample 3701 in Figure 1a. This stands in stark contrast to the phyllosilicate-rich right part of the band (11% and 0.46 md) where permeability has been reduced by almost three orders of magnitude (Figures 1a, 2). Grain-size distributions for the host rock and from within the phyllosilicate-poor left part of the band are almost identical, suggesting that this part of the band is a (noncataclastic) disaggregation structure (Figure 1b). We have not analyzed the grain size in the phyllosilicate-rich part of the band (Figure 1b), but no evidence of cataclasis is observed in this part of the band either.

The second example is from the Entrada Sandstone of the San Rafael Desert, Utah. The approximate burial depth at the time of deformation was around 3 km (1.8 mi) (Aydin, 1978; Davatzes et al., 2003). The sampled sandstone is fine grained, well sorted, and exhibits dissolution at quartz grain-contact points within the band (sample UT-A in Figure 1a). However, thin-section studies have not revealed any quartz overgrowth in this sample. Furthermore, the microstructure of the band is different from the classical deformation bands studied by Aydin, (1978) at the same locality. Because of the dissolution and mild cataclasis in the band, the grain size as well as porosity and permeability have been reduced (Figures 1a, b; 2).

The grain-size distributions along the band are almost identical, except for location number 2, which belongs to the thickest part of the band and has the lowest porosity (Figure 1a, b). Also, the estimated permeability changes along this band. The permeability contrast to the adjacent host rock ranges from one order (minimum reduction) to three orders of magnitude, as shown in Figures 1a and 2. Apart from location number 2 in the band, the porosity and permeability changes do not correlate with variations in band thickness; e.g., location numbers 5 and 6 show approximately the same

(a)

1: 21%, 210 md 2: 22%, 133 md 3: 17%, 38 md 4: 14%, 5 md 5: 15%, 31 md 6: 10%, 8 md 7: 11%, 0.46 md 8: 26%, 87 md

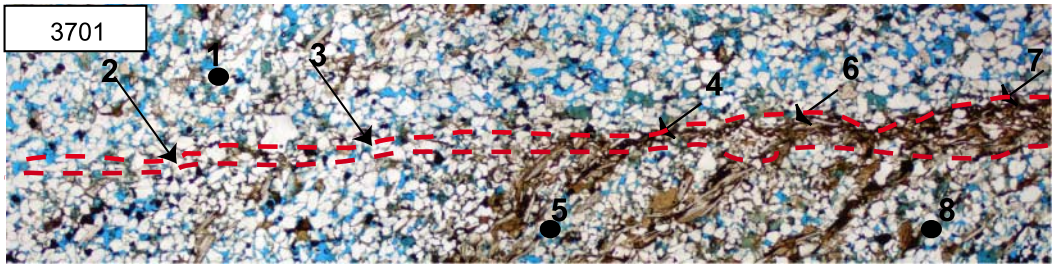

1: 12%, 10 md 2: 10%, 6 md 3: 13%, 12 md 4: 20%, 9 md 5: 28%, 369 md 6: 14%, 5 md 7: 27%, 1359 md

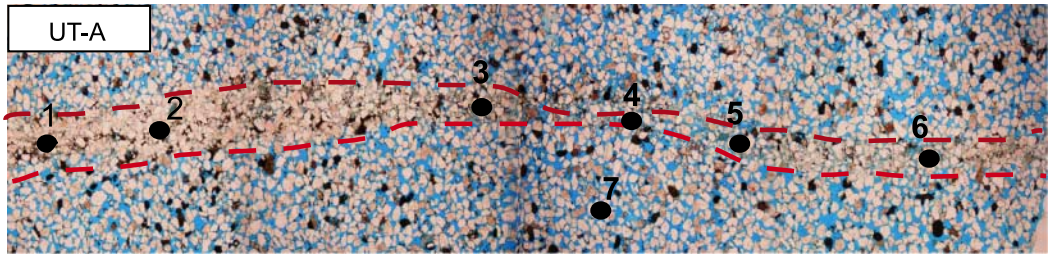

1:6%, 1.7 md 2: 15%, 8 md 3: 15%, 4 md 4: 16%, 6.4 md 5: 15%, 4 md 6: 30%, 8945 md

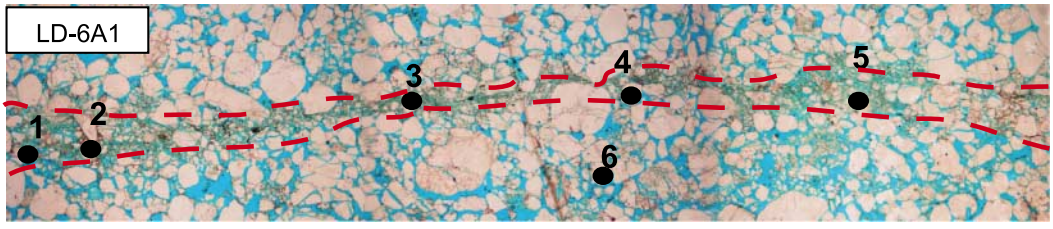

1: 31%, 701 md 2: 20%, 31 md 3: 15%, 14 md 4: 30%, 578 md 5: 26%, 4864 md

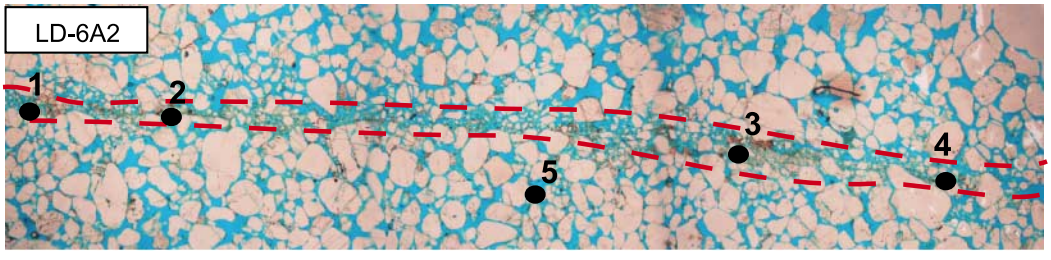

1: 18%, 6.6 md 2: 17%, 4 md 3: 28%, 7.8 md 4: 26%, 8.7 md 5: 20%, 12 md 6: 26%, 141.8 md 7: 27%, 673 md 8: 30%, 19,157 md

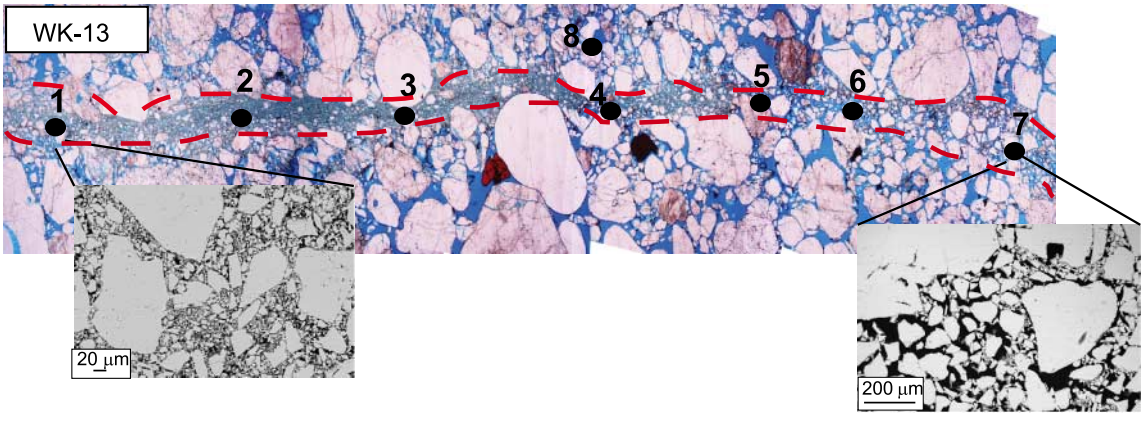

1 mm

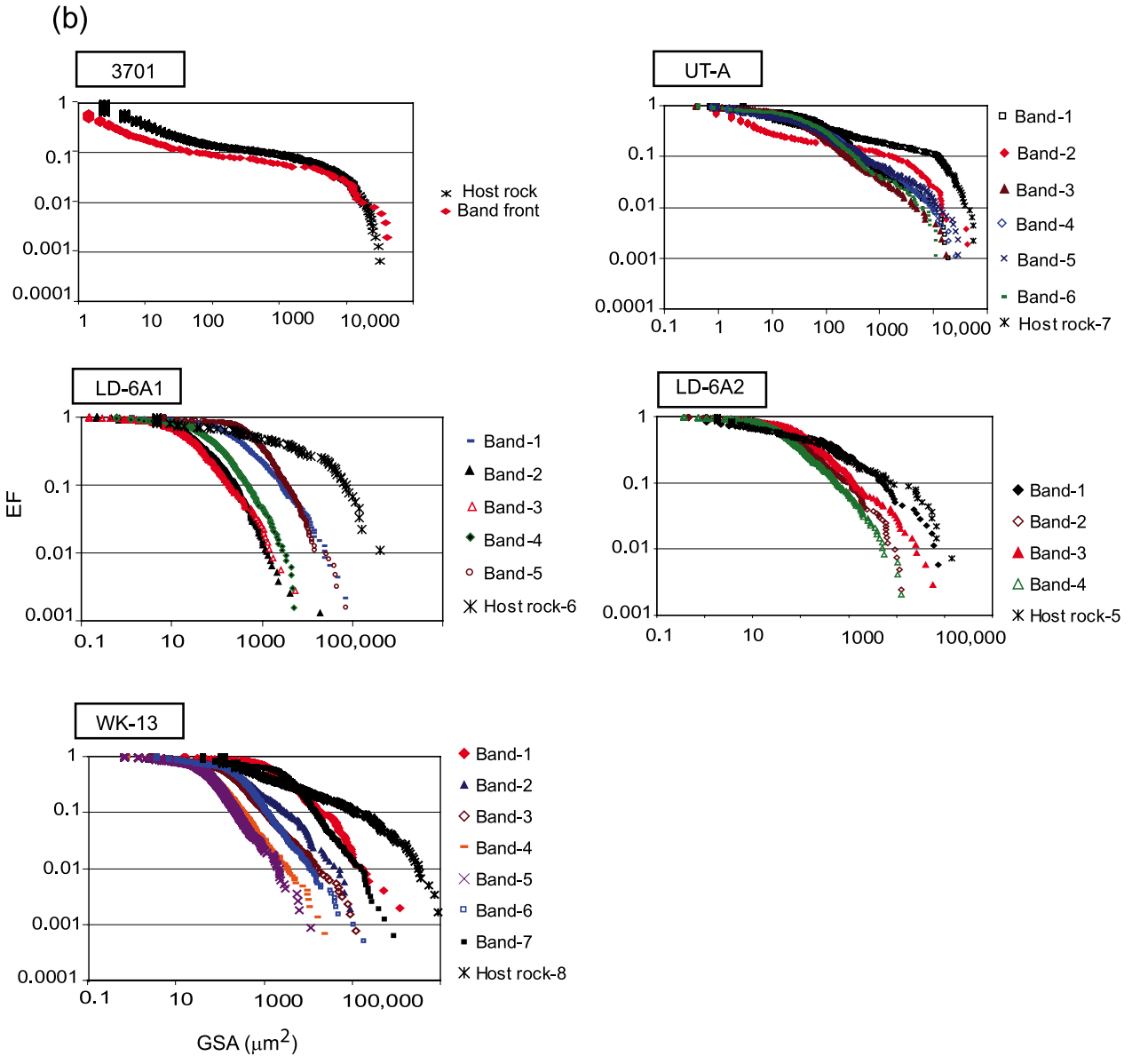

Figure 1. (a) Photomicrographs of thin sections of deformation bands; epoxy saturating the pore space is blue, and porosity and permeability values for measured locations are presented on the top of each picture. On each photograph, the locations are noted by numbers and circles. The numbers on the thin-section images correspond to the numbers used in the presentation of the porosity and permeability data and grain-size distributions. Porosity and permeability were calculated by processing of high-resolution BSE images of the selected locations presented schematically by points on the photomicrographs. Sample 3701 shows a disaggregation or phyllosilicate band; sample UT-A shows a dissolution band; samples LD-6A1 and LD-6A2 and WK-13 show cataclastic bands. Note the selected locations in the beginning and end of band WK-13 (locations 1 and 7), which show similar thickness, but the grain-size distribution, porosity and, permeability values are different. High-magnification BSE images (small pictures attached to this image) reveal different microstructures and grain-size distributions for these two parts, implying different degrees of cataclasis. (b) Exceedance frequency (EF) plot of the grain-size area (GSA) for all of the presented samples in panel a.

thickness whereas location 5 has a porosity value twice that of number 6 and a permeability that is higher by two orders of magnitude (Figure 1a).

The third and fourth thin-section examples (samples LD-6A1 and LD-6A2) are from medium-grained and poorly sorted Nubian Sandstone (Wadi Khaboba, Sinai, Egypt). The maximum burial depth at the time of faulting was about 1.5 km (0.9 mi) (Du Bernard et al., 2002; Rotevatn et al., 2008). Both thin sections were prepared perpendicular to each

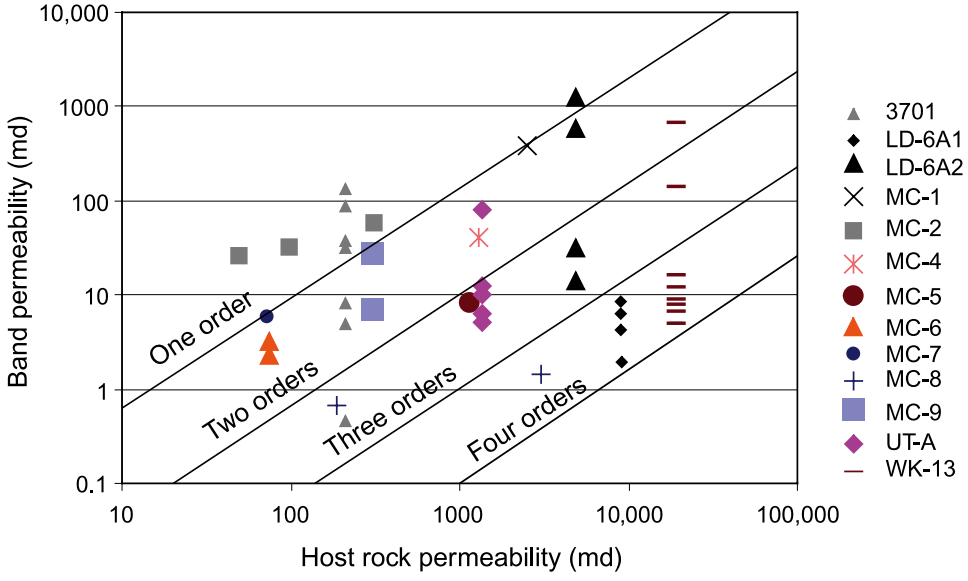

Figure 2. Plot of calculated permeability values within deformation bands versus host-rock permeability. Note the reductions in permeability by up to four orders of magnitude in the deformation bands.

other from the same sample. They show variation in microstructure along the band in both directions, related to the intensity of cataclasis and amount of iron oxide cement. This affects the grain-size distributions, porosity, and permeability (Figure 1a).

For the host rock, differences in grain-size distributions between LD-6A1 and LD-6A2 are observed (Figure 1b). The estimated host-rock porosity and permeability in LD-6A1 are 30% and 8945 md, respectively, whereas the corresponding values for LD-6A2 are lower (26% and 4864 md, respectively). Minimum porosity and permeability are found in a part of band LD-6A1 characterized by intense cataclasis and iron oxide cement (6% porosity and 1.7 md permeability). In the rest of the band (LD-6A1), porosity does not change, and permeability changes are small. Overall porosity and permeability inside the band are lower in LD-6A1 than in LD-6A2, which is likely related to more intense cataclasis in LD-6A1 (Figure 2). Both porosity and permeability change along the band in LD-6A2, but permeability changes are higher, ranging from 14 to 1238 md, i.e., a variation of two orders of magnitude (Figures 1a, 2). In contrast to petrophysical properties, band thickness remains almost constant for the LD-6A2 sample. Moreover, the changes in thickness of the band in LD-6A1 do not correspond to the degree of cataclasis and petrophysical properties measured along the band.

The fifth and last example is from a medium- to coarse-grained and poorly sorted version of the Nubian Sandstone from Sinai, Egypt (sample WK-13 in Figure 1a). This sample is from the same locality as samples LD-6A1 and LD-6A2 in Figure 1a but shows intensive cataclasis and grain-size reduction that vary along the band (Figure 1a, b). The permeability has been reduced by up to four orders of magnitude (Wk-13) from a very high permeability in the host rock (19,157 md) down to 4 md within the band (Figure 2). The porosity changes from a maximum of 30% in the host rock to 17% within the band (Figure 1a). Porosity and permeability measurements also show variations along the band with ranges from 28 to 17% and from 673 md down to 4 md, respectively (Figure 1a).

The grain-size analyses show a reduction of the grain-size area in the band compared to the host rock (Figure 1b), although the grain-size area varies also along the band. Again, the thickness variation does not correlate with the change in microstructure and petrophysical properties (Figure 1a). This is shown by the fact that the selected locations in the beginning and end of the band (locations 1 and 7) show similar thickness, but the grain-size distribution, porosity, and permeability values are different. High-magnification BSE images (Figure 1a) reveal different microstructures and grain-size distributions for these two parts, implying a different degree of cataclasis.

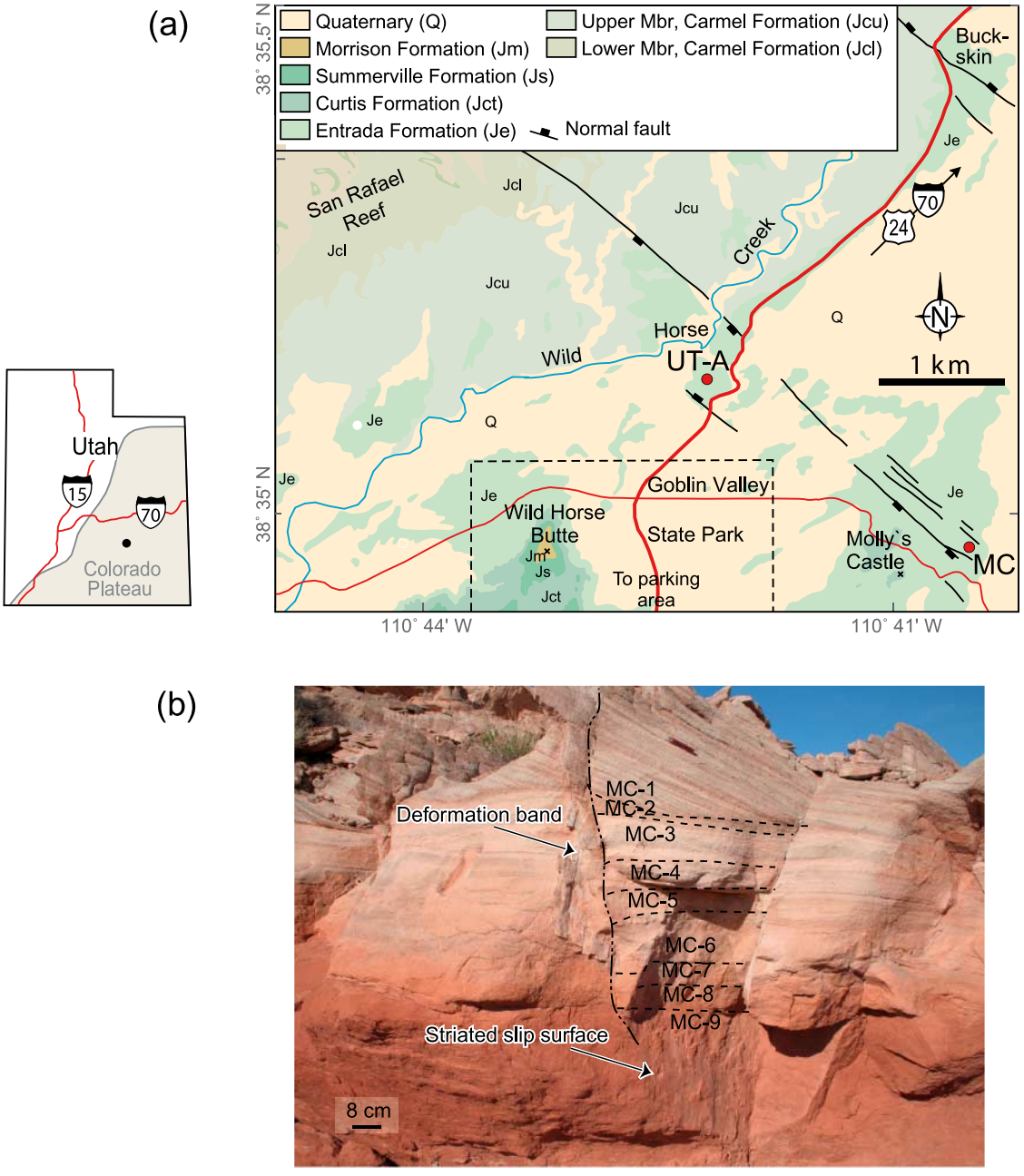

Figure 3. (a) Geologic map showing the studied locality (MC) in the San Rafael Desert, Utah, and the location for sample UT-A. Modified from Doelling (2001). (b) A picture from the locality where the MC samples were taken.

Effect of Initial Grain Size and Porosity

The influence of initial grain size and porosity of the host rock on the development of deformation band microstructure and properties was explored through a study of deformation bands that cross nine definable layers at the base of an eolian sand unit in the Entrada Sandstone in the San Rafael Desert, Utah (Figure 3). The burial depth is estimated to be about 3 km (1.8 mi) at the time of deformation (Aydin, 1978; Davatzes et al., 2003). The grain size is generally fining upward through these layers, but detailed analyses show the grain size and porosity to change at the scale of a single thin section (Figures 4, 5).

In the upper layer (MC-1 in Figures 3, 4a), the sandstone is medium grained and well sorted. The

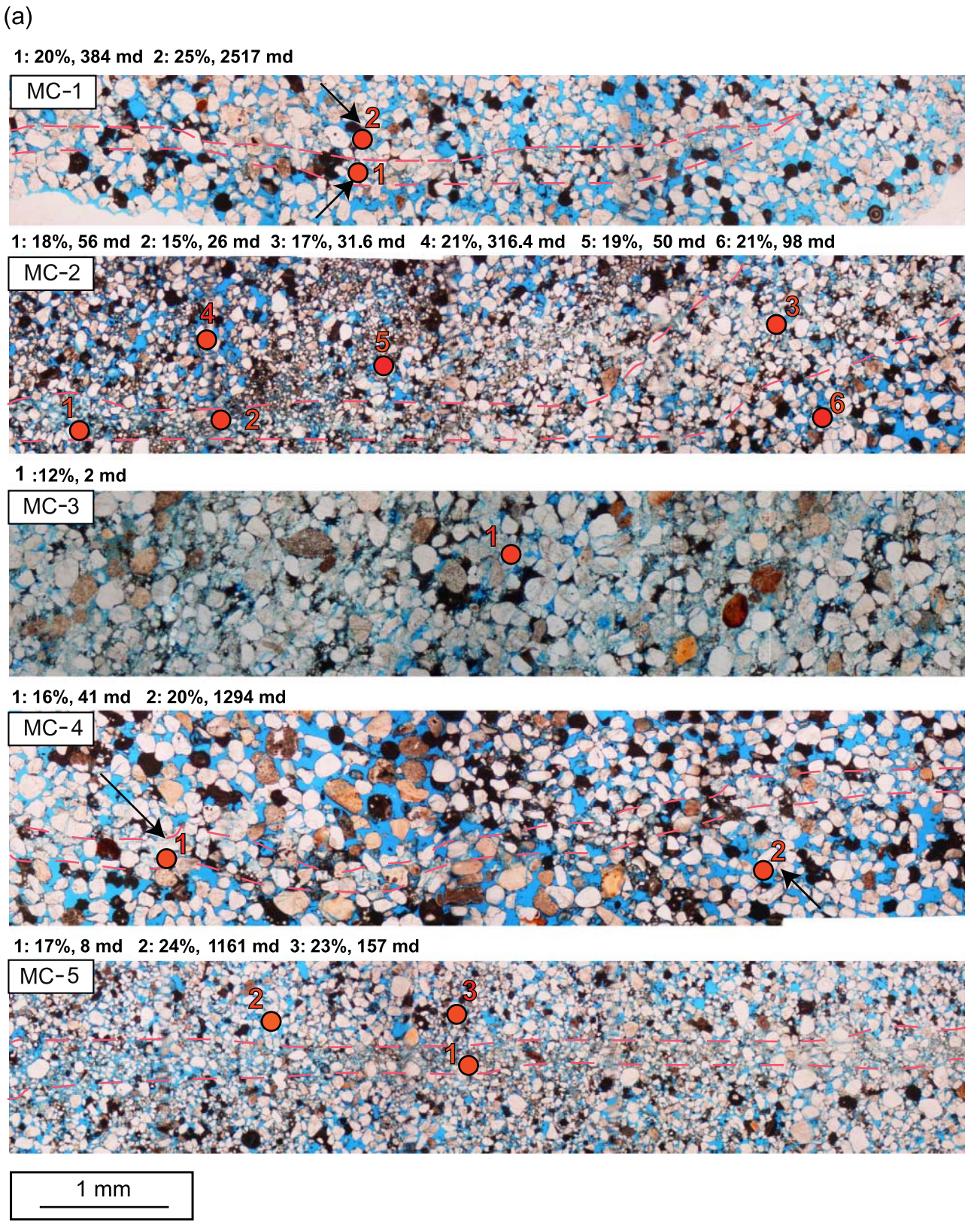

Figure 4. (a) Photomicrographs of MC-1–5 thin sections; epoxy saturating the pore space is blue, and porosity and permeability values for measured locations are presented on the top of each picture. On each photograph, the locations are noted by numbers and circles. The numbers on the thin-section images correspond to the numbers used in the presentation of the porosity and permeability data and grain-size distributions. (b) Exceedance frequency (EF) plot of the grain-size area (GSA) for all of the presented samples in panel a.

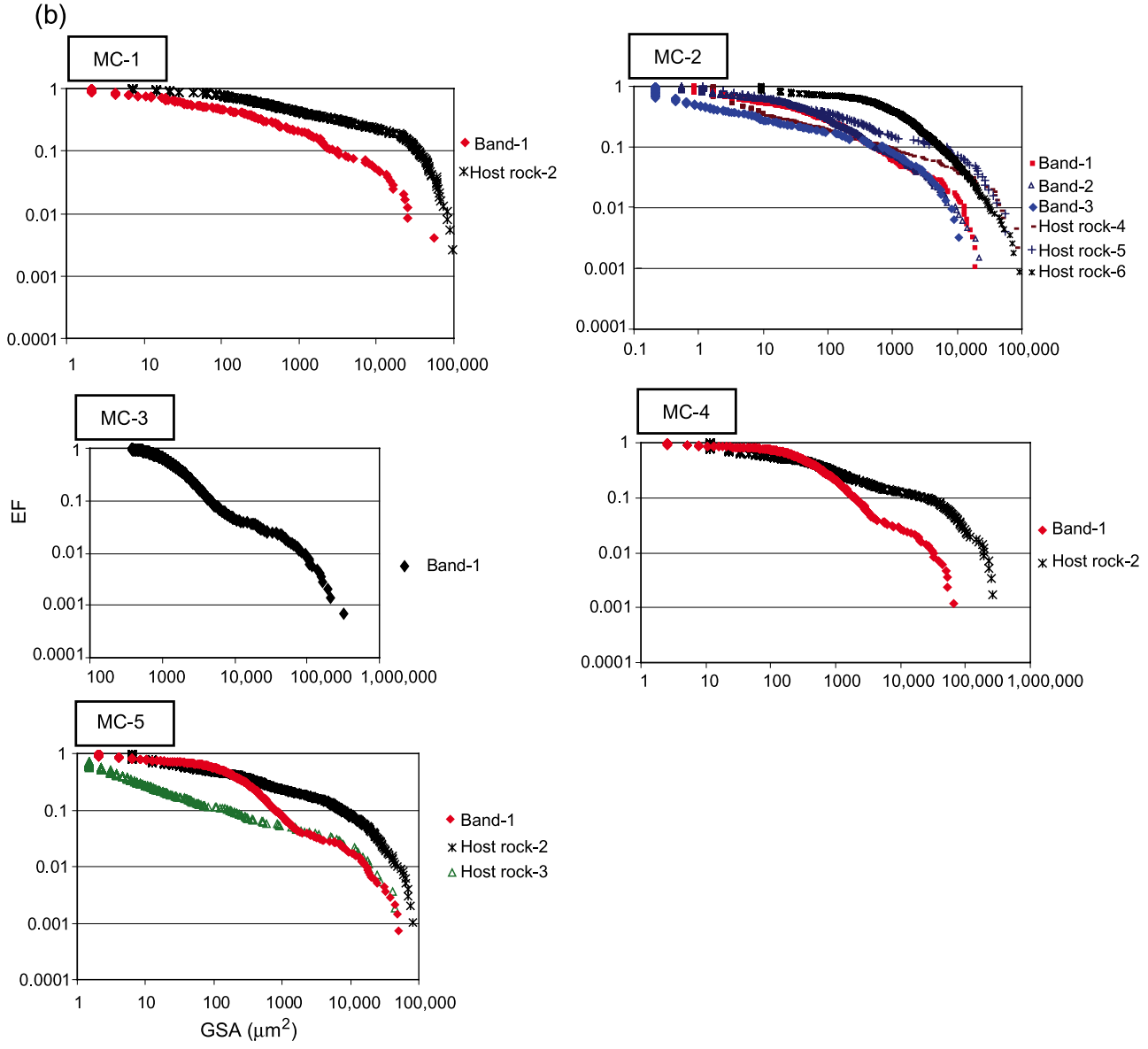

Figure 4. Continued.

grain-size distribution is almost constant in the host rock but somewhat reduced within the band because of mild cataclasis (Figure 4b). The thickness of the band varies, especially on the right side (Figure 4a) where the band is hard to define. Porosity changes from 25% in the host rock to 20% inside the band, whereas permeability decreases from 2517 to 384 md, i.e., about one order of magnitude (Figure 2).

In the thin section from the next layer down (MC-2 in Figures 3, 4a), the host-rock sandstone is very poorly sorted and has several fine-grained laminae. Cataclasis is the main deformation mechanism in this band. Moreover, the presence of the fine-grained host-rock laminae locally reduces the grain-size area of the band and affects porosity and permeability (Figure 4a, b). Porosity and permeability do not change significantly from the fine-grained laminae in the host rock to the parts of the band containing the fine-grained laminae (Figure 4a). In contrast, the permeability of the coarse-grained host rock outside the band is one order of magnitude higher than the corresponding part of the band (Figures 2, 4a). Tracing the band

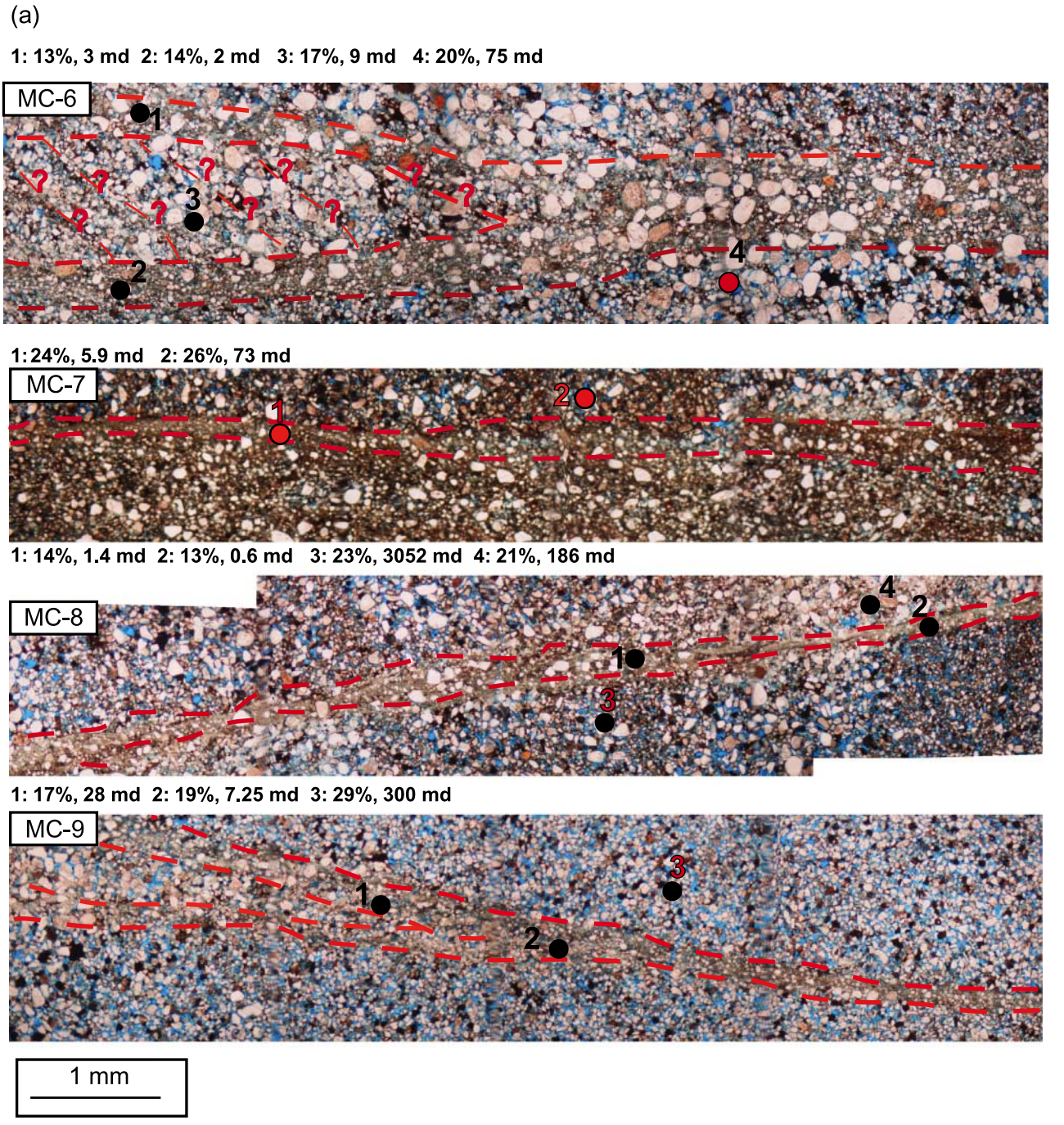

Figure 5. Same as Figure 4, but for samples MC-6–9. EF = exceedance frequency; GSA = grain-size area.

on the right side of the section in Figure 4a is not easy, where it seems to appear as a zone of deformation with a somewhat lower porosity and permeability than its surroundings (Figure 4a).

In layer MC-3 (Figure 3), the thin section only shows the deformed sandstone, and therefore, comparing the grain-size area, porosity, and permeability within and outside the band is difficult (Figure 4a). The grain-size distribution is bimodal in that it contains a considerable amount of both fine and coarse grains (Figure 4b). Porosity and permeability are lower than the estimated values from layers MC-1 and MC-2 (Figures 2, 4a), suggesting a higher degree of cataclasis in this sample.

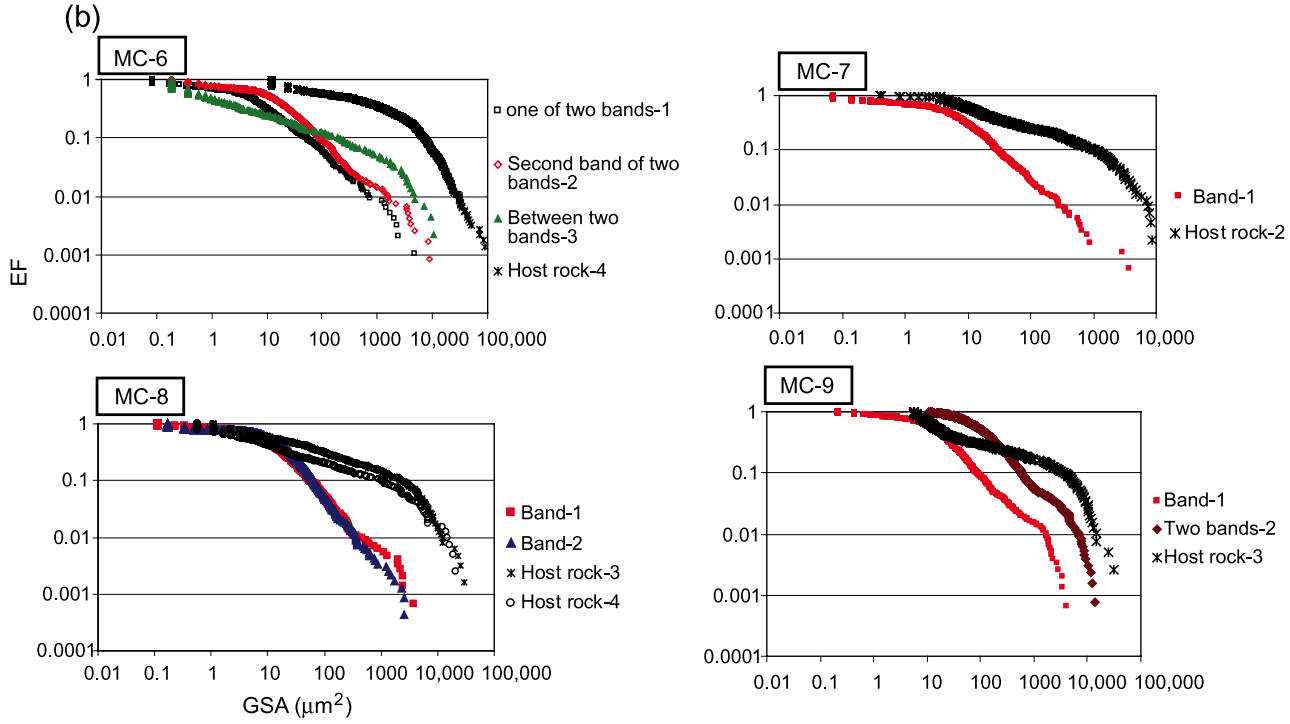

Figure 5. Continued.

The sandstone in the fourth layer (MC-4 in Figure 3) is poorly sorted, and the grain-size distribution both outside and inside the deformation band is bimodal (Figure 4b). Porosity is slightly decreased, whereas permeability is reduced by up to two orders of magnitude within the band, mainly as a result of cataclasis (Figures 2, 4a). The band has a fairly constant thickness.

The thin section from the fifth layer (MC-5 in Figure 3) shows the sandstone to be poorly sorted (Figure 4a). The host rock consists of both coarse- and fine-grained sandstone (see locations 2 and 3). Porosity is slightly higher in the coarse-grained host rock, but permeability is significantly higher in location 3. The band shows a fairly constant thickness, and the grain-size analysis reveals a bimodal distribution and also grain-size reduction in the band (Figure 4b). This reduction is related to the low to moderate amount of cataclasis. Similar to the previous bands, small porosity changes are observed, whereas permeability varies up to three orders of magnitude (Figures 2, 4a).

In the thin section from layer MC-6 (Figure 5a), two branching bands in the left part exist. The thin section shows a very poorly sorted sandstone with finer grain-size areas around two bands. However, the grain-size distributions along these bands are identical (Figure 5b). The highest permeability reduction in these bands is one order of magnitude (Figure 2). Porosity decreases from 20% down to 13 and 14% within the bands (Figure 5a). The bands in this layer also show evidence of cataclasis.

The thin section from layer MC-7 (Figure 5a) portrays a poorly sorted sandstone with a high content of iron oxide cement. The grain size has obviously been reduced by cataclasis in this band (Figure 5b). Furthermore, porosity is reduced slightly, and permeability is reduced by one order of magnitude compared to the host rock (Figure 2).

In the sample from layer MC-8 (Figure 3), the sandstone is seen to be poorly sorted (Figure 5a). The boundaries of the band are sharp and well defined in the BSE images, which can be related to the intense cataclasis in this band. The grain-size analysis (Figure 5b) shows two different grain-size distributions in the host rock. The one obtained from location 4 is finer than that from location 3 in Figure 5a. As expected, porosity and permeability

are higher in the coarse host rock than in the fine one. Two measured locations in the band show almost similar thickness, grain-size distribution, and porosity, whereas permeability is one order of magnitude lower in location 2 than location 1 (Figures 2; 5a, b).

In the section from layer MC-9, two bands merge to form a single thin band (Figure 5a). The sandstone is fine grained and poorly sorted. The grain-size area is finer in the merged bands than in the individual branches (Figure 5b). Porosity decreases by up to 12% in the band as compared to the host rock (Figure 5a). Permeability decreases by up to two orders of magnitude into the band (Figures 2, 5a).

DISCUSSION

Most previous workers address deformation bands and the reduction in permeability across them through plug and minipermeameter measurements. In this work, we have demonstrated very significant spatial variations in porosity and permeability along deformation bands by using backscatter image processing and microtextural investigations. We also demonstrated that these variations occur in several types of deformation bands, i.e., bands dominated by various types of brittle and ductile deformation mechanisms. Hence, the reasons for these variations may be different for different types of deformation bands.

Band Thickness

Experimental and numerical studies show that the thickness of shear deformation bands depends on grain size, grain angularity, initial density, and confining pressure (Haied et al., 2000; Bésuelle, 2001; El Bied et al., 2002; Alsaleh et al., 2006; Alshibli et al., 2006). The presence of coarse, nonfractured grains in the bands, e.g., the intact coarse grain in each of the bands in Figure 1a, affects the thickness of the bands. The presence of intact coarse grains in the middle of cataclastic bands can be explained by the fact that selective fracturing of relatively large grains is favored at high confining pressures during shearing (Blenkinsop, 1991). For the examples presented here, the confining pressure may not be sufficient to cause the fracturing of the largest grains. In other words, the grain comminution within cataclastic bands has not reached the steady-state particle-size distribution (Sammis et al., 1987; Torabi et al., 2007). Our observations also show that the band is thicker where the mica content is high in the phyllosilicate band (Figure 1a).

Numerical modeling of strain localization in granular material shows that shear band thickness tends to decrease as a result of increasing confining pressure (Alsaleh et al., 2006; Alshibli et al., 2006). Furthermore, the results from ring-shear experiments reveal that increasing the level of normal stress (corresponding to confining pressure) can change shear-zone boundaries from diffuse to sharp, implying a reduction in their thickness (Torabi et al., 2007). In this light, the natural deformation bands studied here may be expected to have formed at different confining pressures. However, for each band, the confining pressure and bulk strain are basically constant at the scale of observation during the formation of the deformation bands. Hence, the variations in microtexture and degree of cataclasis along the bands can be better ascribed to variations in strain within the bands; i.e., stronger strain localization implies more cataclasis. The inherent mineralogical and physical weaknesses of the grains that are targeted to strain localization control their modes of fracturing and might influence the local variation in thickness along deformation bands. For example, at shallow to medium burial depth, the relative grain strength of rock fragment and feldspar is lower than quartz (Rawling and Goodwin, 2003), which results in transgranular fracturing of the formers. This increases strain softening (localization) and consequently decreases the thickness of the band. However, in some of the studied samples, the level of strain localization is not simply related to the thickness of the band. For instance, the two selected parts of the band in sample WK-13 in Figure 1a have almost the same thickness but show different degrees of cataclasis and hence different grain-size and petrophysical properties.

Deformation Mechanism

Initial porosity and grain size are important factors influencing the deformation mechanism (Wong et al., 1997; Flodin et al., 2003). The MC Entrada samples all show clear evidence of cataclasis, but the grain-size analyses indicate that the degree of cataclasis changes from one layer to the next. This change can be related to different initial porosity and grain size in the different host-rock layers (Figures 4, 5).

The effect of phyllosilicate and cement content on deformation mechanism during the deformation of granular material has received some attention (e.g., Trent, 1989; Yin and Dvorkin, 1994; Flodin et al., 2003). As phyllosilicate deforms in a ductile instead of a brittle manner, no evidence of cataclasis in the studied phyllosilicate band is seen (sample 3701 in Figure 1a). The porosity and permeability reduction found in the phyllosilicate band in Figure 1a depends on the local phyllosilicate content of the band and hence the variations in phyllosilicate in the host rock: the porosity and permeability values are lower where the band has higher phyllosilicate content. This is well illustrated by location number 7 in Figure 1a, which has 11% porosity and 0.4 md permeability. This example agrees with previous findings that phyllosilicate content controls the permeability across disaggregation bands (e.g., Fisher and Knipe, 2001).

Cemented granular material is found to be more resistant to grain crushing as compared to the same uncemented material for the same loading and confining pressure (e.g., Trent, 1989; Yin and Dvorkin, 1994). Quartz dissolution and iron oxide cement in deformation bands hinder cataclasis by increasing the bounding surface of the grains and hence distributing the contact forces over a larger area (e.g., bands UT-A, LD-6A1, LD-6A2, and WK-13 in Figure 1a). However, iron oxide also can reduce the friction between grains, promoting grain-boundary sliding (Underhill and Woodcock, 1987).

The timing of deformation relative to any chemical dissolution and cementation is also important. Dissolution and cementation decrease porosity and permeability in the band (Figures 1, 4, 5), and postdeformational dissolution can clearly vary along the band. Our observations of sample UT-A (Figure 1a) show that dissolution hinders cataclasis, and thereby, the mild cataclasis in the studied dissolution bands makes its microstructure different from classical deformation bands reported from the same area in the San Rafael Desert, Utah, provided that the dissolution is not postkinematic.

We have investigated the relationship between porosity and permeability in the cataclastic deformation bands and their host rock. Comparing the porosity-permeability data for the cataclastic deformation bands investigated in this study (regardless of the effect of mineralogical differences in the host rocks, Figure 6a) shows a clear relationship between the two. The relationship between porosity and permeability is less well defined for host-rock data (Figure 6a), but a comparison indicates that host-rock permeability is higher than the deformation band permeability for the same porosity value. Although more data would be needed to quantify this difference, it can be explained in terms of the different processes involved: the microstructure of the host rock is controlled by sedimentary processes and compaction, whereas that of the cataclastic bands is very much the result of grain crushing, which results in more angular grains and a different grain-size distribution (Figures 1, 4, 5). As a consequence of cataclasis, the specific surface area of pore-grain interface increases (s, specific surface area is calculated from equation 3 in the Methodology section, see Figure 6b). Therefore, the increase in specific surface area causes more reduction in permeability.

Our study opens new horizons into a detailed understanding of the permeability structure of deformation bands. To understand the relationship between deformation mechanisms within deformation bands on one hand and their microstructure and petrophysical properties on the other, we need to study appropriate experimental and numerical analogs. Studies of other types of deformation bands, such as dilation and compaction bands, have to be performed to be able to estimate or predict variations in petrophysical properties along deformation bands in a variety of settings.

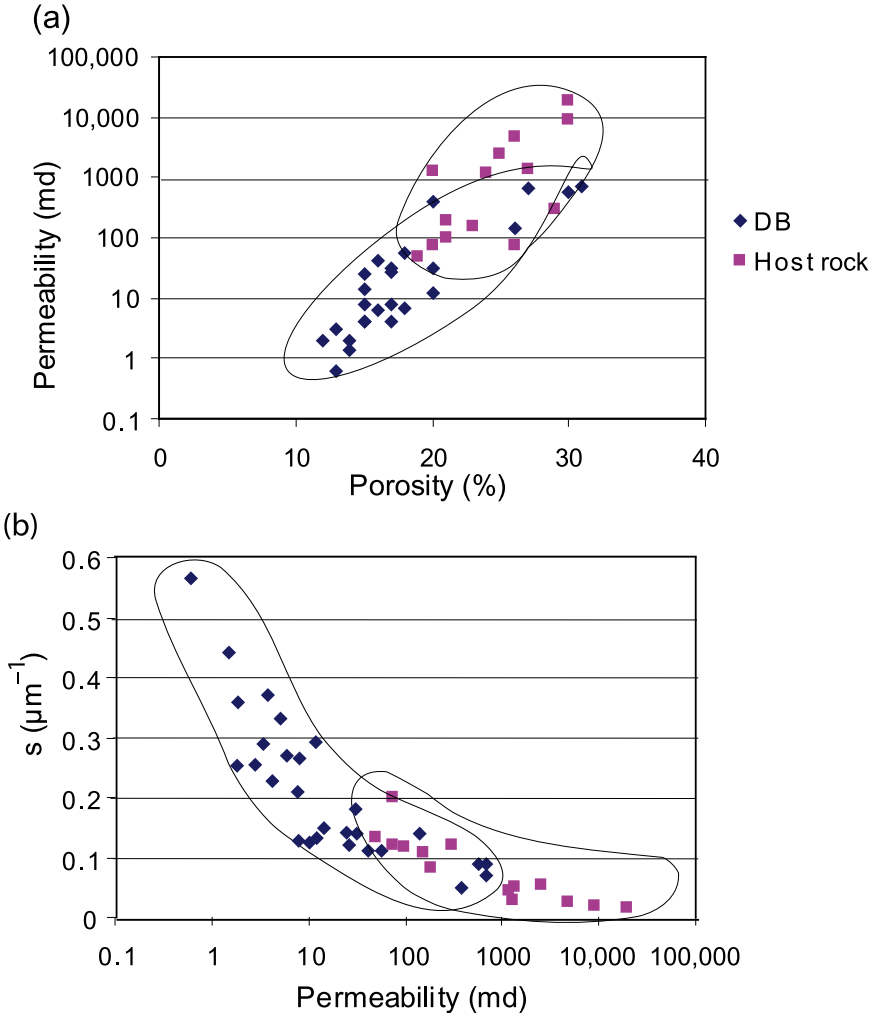

Figure 6. (a) Porosity-permeability relationships for all of the studied cataclastic deformation bands (DBs) and their host rock. (b) Relationship between *s* (specific surface area of the pore-grain interface) and permeability for the deformation bands and their host rock. A higher specific surface area implies lower permeability values. Note the different trends for bands and the host rocks in both plots.

Comparison of Laboratory and In-Situ Measurements of Permeability to Image-Based Calculated Data

We have compared our calculated permeability data to both laboratory measurements on core plugs and in-situ measurements by minipermeameter. Gas permeability was measured on the plugs perpendicular to deformation bands. The minipermeameter data have been mostly measured parallel to the bands because of difficulties in the field. Figure 7 illustrates the permeability data obtained from three different approaches for cataclastic bands near Goblin Valley, Utah. The results show that image-based data lie between minipermeameter and plug-measured values. The difference is higher for the deformation bands than their host rocks because deformation bands show more heterogeneity in their microstructure and because the details of this heterogeneity are not captured by minipermeameter and plug measurements. However, we have derived permeability data from plug measurements from clusters of cataclastic bands in the same locality in Utah that are lower than any other measurements shown in Figure 7. The reason for these low values is that a cluster of deformation bands contains several deformation bands such that their cumulative properties contribute to the obtained permeability value.

The difference between plug and minipermeameter data and our calculated permeability can be explained by the sample-size limitation inherent to the plug and uncertainties associated with the

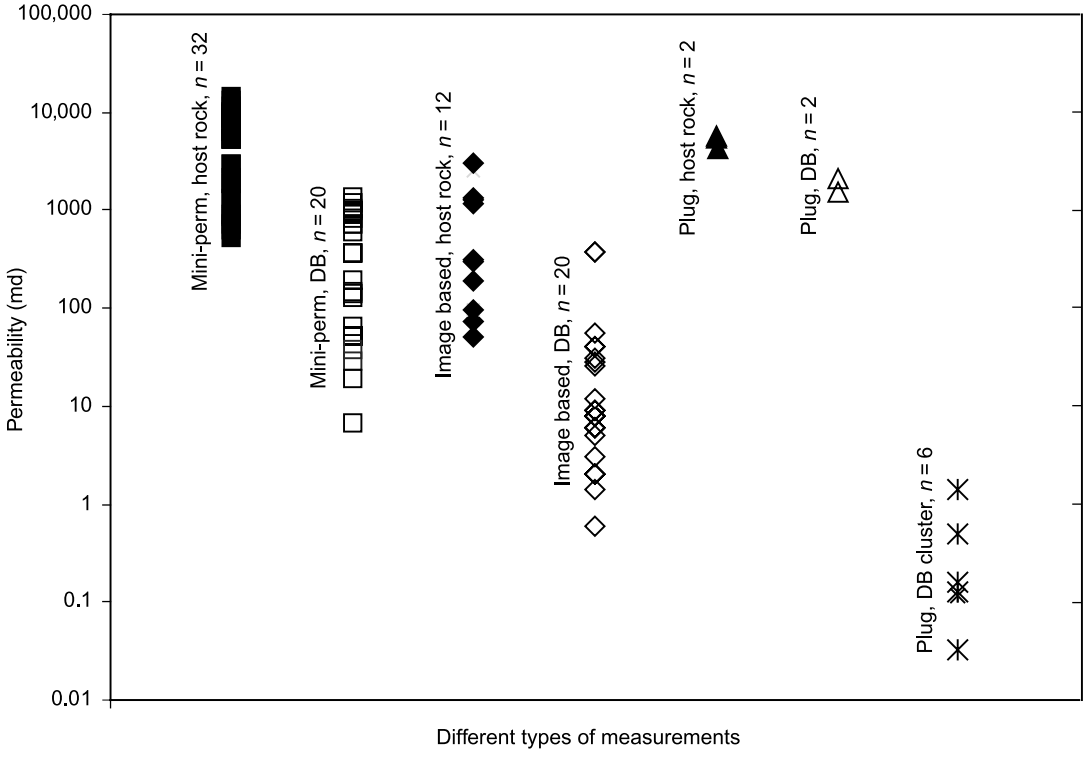

Figure 7. Comparison of permeability values obtained from different approaches (plug, minipermeameter [mini-perm] and image-based measurements). Data are from cataclastic deformation bands (DB) in Goblin Valley. Note that data for clusters of deformation bands show lower permeability values; *n* denotes the number of measurements.

in-situ minipermeameter measurements, which makes it difficult or impossible to get the accurate properties of a millimeter-thick deformation band. The plug and minipermeameter data represent the combined properties of the band and its host rock. Although using image processing methods, we are able to select the area of interest on an image of the thin section and make more precise measurements of porosity and permeability. In the results presented in Figure 2, we show that deformation bands can decrease permeability by up to four orders of magnitude, meanwhile, within a single band, this value can change greatly in a short distance.

Implications for Fluid Flow in Petroleum Reservoirs

Variations in petrophysical properties along deformation bands determine their function in a petroleum reservoir setting. Deformation bands can act as both conduits and barriers on microscopic scale, although the assessment is based on the latter. The rapid variations in properties along bands even on millimeter and centimeter scale make them leaky, which reduces their contribution to the sealing capacity of faults. However, the deformation bands still represent heterogeneities that increase the sinuosity and tortuosity of fluids running through deformed sandstone in a petroleum reservoir and consequently decrease the total effective permeability of the reservoir. In reservoirs containing abundant deformation bands, such as the Jurassic sandstones of the Colorado Plateau, this may have consequences for well planning and field developments.

The influence of deformation bands on productivity strongly depends on the number of deformation bands (i.e., the cumulative thickness and properties of the bands) and on the pattern of permeability variation along the deformation bands. For instance, the relatively low densities of deformation bands mapped in North Sea reservoirs make them unlikely to be of general concern (Fossen and Bale, 2007). The variation in permeability along deformation bands, and therefore their sealing properties, has not been studied systematically before, and we do not know much about their periodicity and frequency. However, plug permeability measurements across deformation

bands show a large variation in reduction from none to several orders of magnitude even within a single reservoir (Fossen and Bale, 2007, and references therein). We suggest that the lateral variations in porosity and permeability documented through the image analyses in the current work could explain at least some of this scatter, indicating that such variations are common.

Disaggregation bands are effective baffles to fluid flow only if the phyllosilicate content is high and evenly distributed throughout the host rock, which is not generally the case. Hence, the variation in permeability values related to the phyllosilicate content in the band, as exemplified by Figure 1a, can explain the wide variation in reported permeability values for this type of bands (e.g., Fisher and Knipe, 2001). Thus, different types of deformation bands (cataclastic and noncataclastic) show spatial variations in petrophysical properties even at the centimeter scale, suggesting that different factors control these variations in each case. We have demonstrated how variations in mineralogy, notably phyllosilicate content, can cause significant spatial changes in permeability along disaggregation bands. Secondary cementation can also be variably developed, for instance, as a function of clay mineral distribution. The variations documented in cataclastic bands are enigmatic, and more research is required to understand and predict these variations.

CONCLUSIONS

1. Deformation bands in deformed reservoir sandstones can show rapid variations in microstructure that cause variations in porosity and permeability along the bands.
2. These variations occur in disaggregation bands, dissolution or cementation bands, and cataclastic bands. In particular, the local phyllosilicate content controls properties of disaggregation bands in phyllosilicate-bearing sandstones.
3. Our results show that the estimated permeability variation can change from zero to two or three orders of magnitude over a short (millimeter scale) distance within a single band.
4. Phyllosilicate content influences the thickness of the band; i.e., higher phyllosilicate content correlates to thicker bands.
5. No simple relationship between thicknesses and intensity of cataclasis can be detected in the studied cataclastic deformation bands.
6. The porosity-permeability relationship in the cataclastic bands is affected by cataclasis and the resulting reduction in size, sorting, and roundness of the grains caused by this mechanism. Statistically, this results in lower permeability in the band than in undeformed sandstone of identical porosity.
7. The widely scattered distribution of previously reported porosity and permeability data for both phyllosilicate and cataclastic bands is likely caused by the observed lateral variation in petrophysical properties of individual bands. Permeability variations along deformation bands may result in the restricted contribution of the bands to the sealing properties of faults. Therefore, we predict that they have a little influence on hydrocarbon production in most cases.

REFERENCES CITED

Agung, M. W., K. Sassa, H. Fukuoka, and G. Wang, 2004, Evolution of shear zone structure in undrained ring-shear tests: Landslides, v. 1, p. 101–112.

Alsaleh, M. I., K. A. Alshibi, and G. Z. Voyiadjis, 2006, Influence of micromaterial heterogeneity on strain localization in granular materials: International Journal of Geomechanics, v. 6, p. 248–259, doi:10.1061/(ASCE)1532-3641(2006)6:4(248).

Alshibli, K. A., M. J. Alsaleh, and G. Z. Voyiadjis, 2006, Modeling strain localization in granular materials using micropolar theory, numerical implementation and verification: International Journal for Numerical and Analytical Methods in Geomechanics, v. 30, p. 1525–1544, doi:10.1002/nag.534.

Antonellini, M., and A. Aydin, 1994, Effect of faulting on fluid flow in porous sandstones: Petrophysical properties: AAPG Bulletin, v. 78, p. 355–377.

Archie, G. E., 1942, The electrical resistivity log as an aid in determining some reservoir characteristics: Transactions of the American Institute of Mining, Metallurgical and Petroleum Engineers, v. 146, p. 54–62.

Aydin, A., 1978, Small faults formed as deformation bands in sandstone: Pure and Applied Geophysics, v. 116, p. 913–930, doi:10.1007/BF00876546.

Aydin, A., and A. M. Johnson, 1978, Development of faults

as zones of deformation bands and slip surfaces in sandstone: Pure and Applied Geophysics, v. 116, p. 931–942, doi:10.1007/BF00876547.
Aydin, A., and A. M. Johnson, 1983, Analysis of faulting in porous sandstones: Journal of Structural Geology, v. 5, p. 19–31, doi:10.1016/0191-8141(83)90004-4.
Bakke, S., and P. E. Øren, 1997, 3-D pore-scale modeling of sandstones and flow simulations in the pore networks: Society of Petroleum Engineers Journal, v. 2, p. 136–149.
Berryman, J. G., 1985, Measurement of spatial correlation functions using image processing techniques: Journal of Applied Physics, v. 57, p. 2374–2384, doi:10.1063/1.334346.
Berryman, J. G., 1998, Planar spatial correlations, anisotropy, and specific surface area of stationary random porous media: Journal of Applied Physics, v. 83, p. 1685–1693, doi:10.1063/1.366885.
Bésuelle, P., 2001, Evolution of strain localization with stress in sandstone: Brittle and semi-brittle regimes: Physics and Chemistry of the Earth, v. 26, p. 101–106, doi:10.1016/S1464-1895(01)00032-1.
Blair, S. C., P. A. Berge, and J. G. Berryman, 1996, Using two-point correlation functions to characterize microgeometry and estimate permeabilities of sandstones and porous glass: Journal of Geophysical Research, v. 101, p. 20,359–20,375.
Blenkinsop, T. G., 1991, Cataclasis and process of particle size reduction: Pure and Applied Geophysics, v. 136, p. 59–86, doi:10.1007/BF00878888.
Brace, W. E., 1977, Permeability from resistivity and pore shape: Journal of Geophysical Research, v. 82, p. 3343–3349, doi:10.1029/JB082i023p03343.
Davatzes, N. C., A. Aydin, and P. Eichhubl, 2003, Overprinting faulting mechanisms during the development of multiple fault sets in sandstone, Chimney Rock fault array: Tectonophysics, v. 363, p. 1–18, doi:10.1016/S0040-1951(02)00647-9.
Davis, G. H., 1999, Structural geology of the Colorado Plateau region of southern Utah, with special emphasis on deformation bands: Geological Society of America Special Papers, v. 342, p. 1–155.
Doelling, H. H., 2001, Geologic map of the Moab and eastern part of the San Rafael Desert, 300 600 quadrangles, Grand and Emery Counties, Utah, and Mesa County, Colorado: Salt Lake City, Utah, Utah Geological Survey, Geologic Map 180, scale 1:100,000, 1 sheet.
Doyen, P. M., 1988, Permeability, conductivity, and pore geometry of sandstone: Journal of Geophysical Research, v. 93, p. 7729–7740, doi:10.1029/JB093iB07p07729.
Du Bernard, X. D., P. Eichhubl, and A. Aydin, 2002, Dilation bands: A new form of localized failure in granular media: Geophysical Research Letters, v. 29, p. 2176–2179.
Ehrlich, R., S. K. Kennedy, S. J. Crabtree, and R. L. Cannon, 1984, Petrographic image analysis: I. Analysis of reservoir pore complexes: Journal of Sedimentary Petrology, v. 54, p. 1515–1522.
El Bied, A., J. Sulem, and F. Martineau, 2002, Microstructure of shear zones in Fontainebleau Sandstone: International Journal of Rock Mechanics and Mining Sciences, v. 39, p. 917–932, doi:10.1016/S1365-1609(02)00068-0.
Fisher, Q. J., and R. J. Knipe, 2001, The permeability of faults within siliciclastic petroleum reservoirs of the North Sea and Norwegian Continental Shelf: Marine and Petroleum Geology, v. 18, p. 1063–1081, doi:10.1016/S0264-8172(01)00042-3.
Flodin, E., M. Prasad, and A. Aydin, 2003, Petrophysical constraints on deformation styles in Aztec Sandstone, southern Nevada, U.S.A.: Pure and Applied Geophysics, v. 160, p. 1589–1610.
Fossen, H., and A. Bale, 2007, Deformation bands and their influence on fluid flow: AAPG Bulletin, v. 91, p. 1685–1700, doi:10.1306/07300706146.
Fossen, H., J. Hesthammer, T. E. S. Johansen, and T. O. Sygnabere, 2003, Structural geology of the Huldra fault block (Huldra field), northern North Sea: Marine and Petroleum Geology, v. 20, p. 1105–1118, doi:10.1016/j.marpetgeo.2003.07.003.
Fossen, H., R. A. Schultz, K. Mair, and Z. Shipton, 2007, Deformation bands in sandstones—A review: Journal of Geological Society (London), v. 164, p. 755–769, doi:10.1144/0016-76492006-036.
Garboczi, E. J., D. P. Bentz, and N. S. Martys, 1999, Digital images and computer modeling, *in* P. Wong, ed., Methods in the physics of porous media: San Diego, Academic Press, Experimental Methods in the Physical Sciences, v. 35, p. 1–41.
Gibson, R. G., 1998, Physical character and fluid-flow properties of sandstone-derived fault zone: Geological Society (London) Special Publication 127, p. 83–97.
Haied, A., D. Kondo, and J. P. Henry, 2000, Strain localization in Fontainebleau Sandstone: Mechanics of Cohesive-Frictional Materials, v. 5, p. 239–253, doi:10.1002/(SICI)1099-1484(200004)5:3<239::AID-CFM97>3.0.CO;2-J.
Hesthammer, J., and H. Fossen, 2001, Structural core analysis from the Gullfaks area, northern North Sea: Marine and Petroleum Geology, v. 18, p. 411–439, doi:10.1016/S0264-8172(00)00068-4.
Hesthammer, J., P. A. Bjørkum, and L. Watts, 2002, The effect of temperature on sealing capacity of faults in sandstone reservoirs: Examples from the Gullfaks and Gullfaks Sør fields, North Sea: AAPG Bulletin, v. 86, p. 1733–1751.
Jamison, W. R., and D. W. Stearns, 1982, Tectonic deformation of Wingate Sandstone, Colorado National Monument: AAPG Bulletin, v. 66, p. 2584–2608.
Johansen, T. E. S., and H. Fossen, 2008, Internal deformation of fault damage zones in interbedded siliciclastic rocks, *in* C. A. J. Wibberley, W. Kurtz, J. Imber, R. E. Holdworth, and C. Collettini, eds., The internal structure of fault zones: Implications for mechanical and fluid-flow properties: Geological Society (London) Special Publication 299, p. 35–56.
Keehm, Y., T. Mukerji, and A. Nur, 2004, Permeability prediction from thin sections: 3-D reconstruction and Lattice-Boltzmann flow simulation: Geophysical Research Letters, v. 31, p. 1–4.
Keehm, Y., K. Sternlof, and T. Mukerji, 2006, Computational estimation of compaction band permeability in sandstone: Geosciences Journal, v. 10, no. 4, p. 499–505, doi:10.1007/BF02910443.
Knipe, R. J., Q. J. Fisher, M. R. Clennell, A. B. Farmer, A. Harrison, B. Kidd, E. McAllister, J. R. Porter, and

E. A. White, 1997, Fault seal analysis: Successful methodologies, application and future directions, *in* P. Møller-Pedersen and A. G. Koestler, eds., Hydrocarbon seals: Importance for exploration and production: Norwegian Petroleum Society Special Publication 7, p. 15–40.

Koplik, J. C., and L. M. Vermette, 1984, Conductivity and permeability from microgeometry: Journal of Applied Physics, v. 56, p. 3127–3131, doi:10.1063/1.333872.

Ogilvie, S. R., and P. W. J. Glover, 2001, The petrophysical properties of deformation bands in relation to their microstructure: Earth and Planetary Science Letters, v. 193, p. 129–142, doi:10.1016/S0012-821X(01)00492-7.

Pittman, E. D., 1981, Effect of fault-related granulation on porosity and permeability of quartz sandstones, Simpson Group (Ordovician) Oklahoma: AAPG Bulletin, v. 65, p. 2381–2387.

Rawling, G. C., and L. B. Goodwin, 2003, Cataclasis and particulate flow in faulted, poorly lithified sediments: Journal of Structural Geology, v. 25, p. 317–331, doi:10.1016/S0191-8141(02)00041-X.

Rotevatn, A., A. Torabi, H. Fossen, and A. Braathen, 2008, Slipped deformation bands: A new type of cataclastic deformation bands in western Sinai, Suez Rift, Egypt: Journal of Structural Geology, v. 30, p. 1317–1331, doi:10.1016/j.jsg.2008.06.010.

Rykkelid, E., and H. Fossen, 2002, Layer rotation around vertical fault overlap zones: Observations from seismic data, field examples and physical experiments: Marine and Petroleum Geology, v. 19, p. 181–192, doi:10.1016/S0264-8172(02)00007-7.

Sammis, C., G. King, and R. Biegel, 1987, The kinematics of gouge deformation: Pure and Applied Geophysics, v. 125, p. 777–812, doi:10.1007/BF00878033.

Sen, P. N., C. Scala, and M. H. Cohen, 1981, A self-similar model for sedimentary rocks with application to the dielectric constant of fused glass beads: Geophysics, v. 46, p. 781–795, doi:10.1190/1.1441215.

Torabi, A., A. Braathen, F. Cuisiat, and H. Fossen, 2007, Shear zones in porous sand: Insights from ring-shear experiments and naturally deformed sandstones: Tectonophysics, v. 437, p. 37–50, doi:10.1016/j.tecto.2007.02.018.

Torabi, A., H. Fossen, and B. Alaei, 2008, Application of spatial correlation functions in permeability estimation of deformation bands in porous rocks: Journal of Geophysical Research, v. 113, p. 1–10.

Trent, B. C., 1989, Numerical simulation of wave propagation through cemented granular material, *in* D. Karamanlidis and R. B. Stout, eds., AMD-101, Wave propagation in granular media: Proceedings of the Winter Annual Meeting of ASME, p. 9–15.

Underhill, J. R., and N. H. Woodcock, 1987, Faulting mechanisms in high porosity sandstones: New Red Sandstone, Arran, Scotland, *in* M. E. Jones and R. M. F. Preston, eds., Deformation of sediments and sedimentary rocks: Geological Society Special Publication 29, p. 91–105, doi:10.1144/GSL.SP.1987.029.01.09.

White, J. A., R. I. Borja, and J. T. Fredrich, 2006, Calculating the effective permeability of sandstone with multiscale lattice Boltzmann/finite element simulations: Acta Geotechnica, v. 1, p. 195–209, doi:10.1007/s11440-006-0018-4.

Wissler, T. M., 1987, Sandstone pore structure: A quantitative analysis of digital SEM images: Ph.D. thesis, Massachusetts Institute of Technology, Cambridge, 564 p.

Wong, P. Z., J. Koplik, and J. P. Tomanic,1984, Conductivity and permeability of rocks: Physics Review, v. 30, p. 6606–6614.

Wong, T.-F., C. David, and W. Zhu, 1997, The transition from brittle faulting to cataclastic flow in porous sandstones: Mechanical deformation: Journal of Geophysical Research, v. 102, p. 3009–3025, doi:10.1029/96JB03281.

Yin, H., and J. Dvorkin, 1994, Strength of cemented grains: Geophysical Research Letters, v. 21, p. 903–906, doi:10.1029/93GL03535.